Final Technical Report

USGS Award G11AP20193

Exploring the Likelihood of Earthquake Ruptures on the San Andreas Fault Breaking Through the San Gorgonio Pass Area by Using Dynamic Rupture Simulation and the Community Fault Model

P.I. Shuo Ma
Department of Geological Sciences
San Diego State University
5500 Campanile Dr.
San Diego, CA 92182-1020

Phone: (619) 594-3091
Fax: (619) 594-4372
Email: sma@mail.sdsu.edu

Term covered by the award: August 15, 2011 – August 14, 2013

Research supported by the U.S. Geological Survey (USGS), Department of the Interior, under USGS award number G11AP20193. The views and conclusions contained in this document are those of the authors and should not be interpreted as necessarily representing the official policies, either expressed or implied, of the U.S. Government.

Abstract

Exploring the likelihood of through-going earthquake ruptures along the complex San Gorgonio Pass (SGP) section of San Andrea Fault (SAF) is of great importance to the seismic hazard assessment in southern California. Previous numerical modeling studies suggested that large northward-propagating events on the SAF that breaks through the SGP will likely result in substantial increase of ground-motion intensity in the greater Los Angeles area. We focus on the physical plausibility of such large through-going rupture scenarios from a mechanical point of view by performing 3-D dynamic rupture simulations. We incorporate realistic fault geometries based on the SCEC Community Fault Model version 4.0. In particular, the Banning Fault in the SGP region is assumed to be the active strand for through-going ruptures. We simulated scenarios of ruptures nucleated from either the San Bernadino (SB) segment of the SAF (north of SGP) or the Coachella Valley (CV) segment of the SAF (south of SGP) to investigate the effects of fault geometry and stress condition on rupture dynamics and ground motions. Initial results from two end-member sets of calculations using different approaches of assigning initial fault traction showed that the fault geometry plays distinctly different roles regarding the plausibility of through-going ruptures in the SGP region depending on the initial fault traction condition: (1) With homogeneous volume stress input and off-fault plasticity, rupture fails to break through the SGP section regardless of propagation direction or speed. In this case, fault geometry dictates the prestress/traction on the fault and has a major effect on rupture dynamics; (2) with heterogeneous fault tractions and pure elasticity, rupture properties seem not to be affected much by the relatively long-wavelength geometric irregularities of the Banning fault as is represented in the CFM-v4. In this case, fault geometry has little effect on rupture dynamics. On the other hand, the ground motion patterns showed clear signatures of the complex fault geometry in all cases.

Publications resulting from this grant include:

Shi, Z., S. Ma, S. M. Day, and G. P. Ely (2012), Dynamic rupture along the San Gorgonio Pass section of the San Andreas Fault, *Seism. Res. Lett*., 83, 423.

Report

In this project we studied the plausibility of a through-going rupture along the San Gorgonio Pass (SGP) section of the San Andreas Fault (SAF) from the perspective of rupture dynamics by performing physics-based 3-D numerical simulations. As revealed by a multitude of geological and geophysical studies, the SGP section is among the most geometrically complex section of SAF, with several possible combinations of fault strands connecting the SB segment to the north and the CV segment to the south (Plesch et al., 2007). The complexity of fault structures in the SGP area poses a great challenge to researchers in answering a long-standing question regarding the possibility of a giant through-going San Andreas rupture. Our dynamic rupture models in the current study adopted a 3-D fault geometry guided by the SCEC Community Fault Model (CFM) version 4 (Plesch et al., 2007) and considered the scenarios of rupture nucleation from north and south of SGP under different initial stress conditions.

Previous observational studies based on geological and geophysical data have revealed a complex combination of right-lateral strike-slip, oblique-slip and thrust faulting on multiple non-vertical fault strands in the SGP region. In the current modeling study, we chose one of the most likely dominant active structures that connect the SB and the CV segment of SAF, viz., the Banning fault, as a single-fault expression of the SAF through the SGP (Fig. 1).

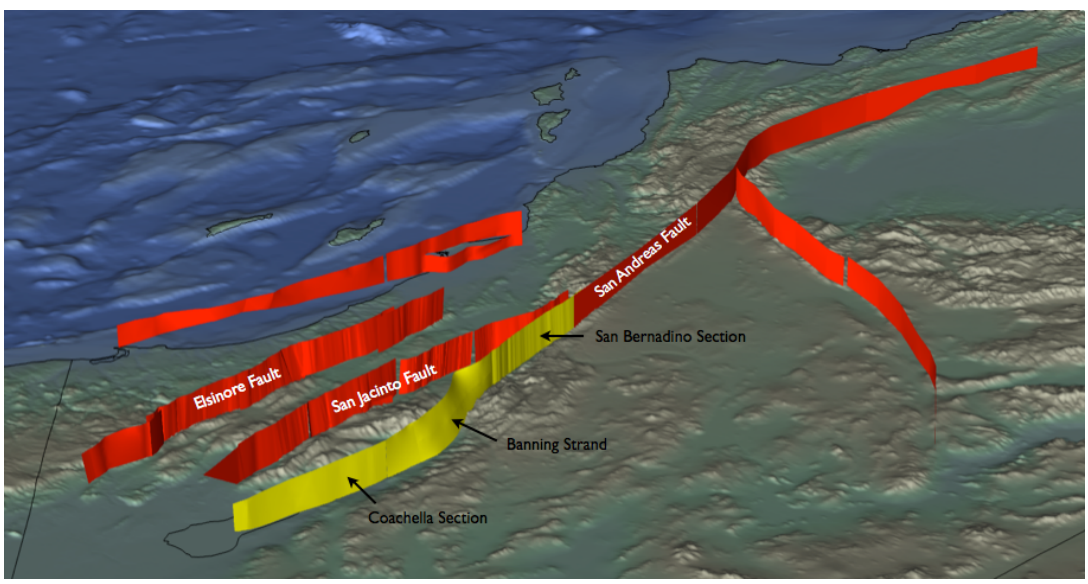

Figure 1. Major faults in Southern California from the SCEC CFM v4. The SAF section in yellow shows the fault geometry adopted in our 3-D dynamic rupture simulations.

In order to concentrate our efforts on exploring effects of fault geometry and initial stress condition, we assumed in our numerical studies flat topography on top and uniform material properties in the bulk (Fig. 2), with density ρ = 3000 kg/m^3, *P*-wave speed α = 6000 m/s and *S*-wave speed β = 3464 m/s. Rupture propagation along the fault is governed by a linear slip-weakening friction with static and dynamic coefficients of friction μ_s = 0.4, μ_d = 0.15 and characteristic slip distance L = 0.1 m. Numerical simulations are carried out using a generalized finite difference code SORD [*Ely et al.*, 2009, 20010; *Shi and Day*, 2013], with an average grid spacing of 100 m in the structured hexahedral mesh employed for model discretization.

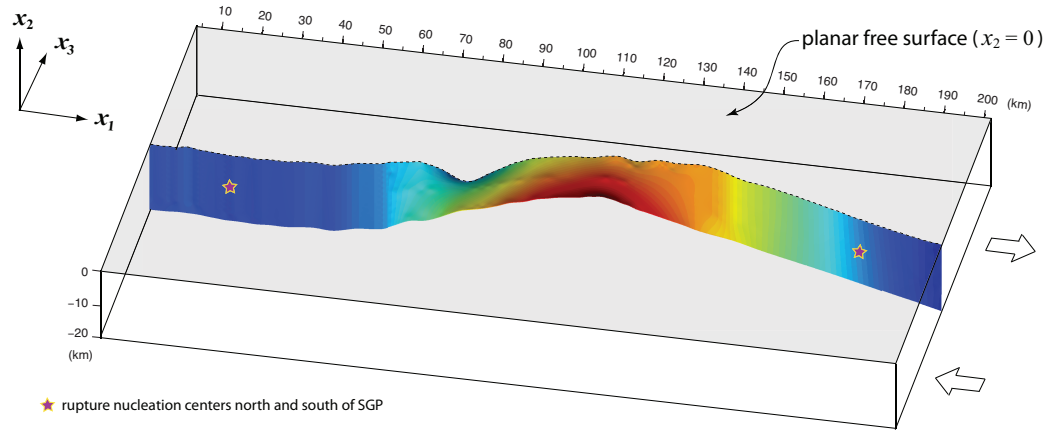

Figure 2. Model geometry, dimensions and coordinate system used in the numerical simulation.

The stress field in southern California region displays a certain degree of inhomogeneity at various scales, partly due to the presence of a complex fault network. Previous observational studies using a variety of datasets, including borehole breakouts, hydraulic fracturing experiments and focal mechanism inversions [e.g., *Townend and Zoback*, 2004], showed that the maximum horizontal compressive stress tends to have a relatively high angle to the local fault strike. To specify initial tractions on the fault, we can either directly assign the traction distribution or indirectly determine it by resolving the immediate volumetric stress field to the fault plane. We carried out two end-member sets of simulations using the aforementioned two approaches for assigning initial fault tractions. For the first set of calculations (hereafter referred to as "Set I"), we use a homogeneous volumetric stress field as the initial stress input. For the second set of calculations (hereafter referred to as "Set II"), we directly assign randomly generated initial tractions on fault and assume pure elasticity in the bulk.

For the Simulation Set I, the assumed initial volumetric stress field $\boldsymbol{\sigma}^0$ is such that the maximum horizontal compressive stress is at 68° to the mean strike of the SB segment north of SGP: $\sigma_{33}^0 = \sigma_{22}^0 = -\rho g h$, $\sigma_{11}^0 = 0.5858\sigma_{22}^0$ and $\sigma_{31}^0 = 0.2\left|\sigma_{22}^0\right|$ (Fig. 3). Drucker-Prager plasticity is adopted for off-fault inelastic response in this simulation set with cohesion c = 5 MPa and internal friction coefficient $\phi = \tan^{-1}(0.75)$.

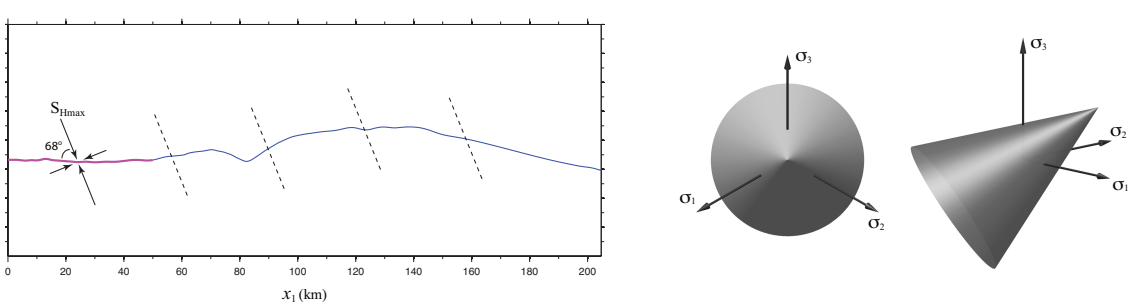

(a) (b)

Figure 3. (a) Map view of the surface fault trace and orientation of the input homogeneous volumetric stress field. The maximum horizontal compressive stress is at a relatively 68° to the mean strike of the SB segment. (b) Yield surface of the Drucker-Prager yield criterion in the 3D space of principal stresses.

The initial distributions of shear traction T_s and normal traction T_n along the fault are obtained by resolving the uniform volumetric stress field onto the non-planar fault. The ratio between the initial shear traction T_s and normal traction T_n reflects the non-planarity of the fault plane (Fig. 4). It has overall large values along the southern segment and very small values along the middle segment in the SGP area (between x_1 = 50 km and x_1 = 115 km).

The spontaneous rupture nucleated on the northern SB segment propagates at subshear speed (top plot in Fig. 5). When the rupture front reaches the edge of the middle low-strength zone at x_1 = ~50 km, it quickly dies out. On the other hand, the spontaneous rupture nucleated on the southern CV segment (bottom plot in Fig. 5) propagates at supershear speed due to large ratio of $|T_s|/|T_n|$. The supershear rupture gradually gets arrested when it enters the middle SGP segment where $|T_s|/|T_n|$ is extremely small.

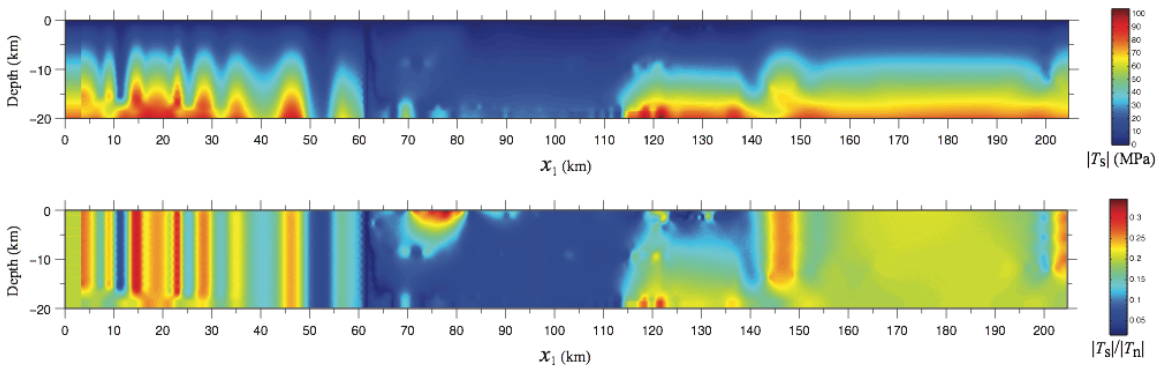

Figure 4. From Simulation Set I: (top) initial shear traction T_s and (bottom) ratio of initial shear traction to initial normal traction $|T_s|/|T_n|$ are projected on a plane.

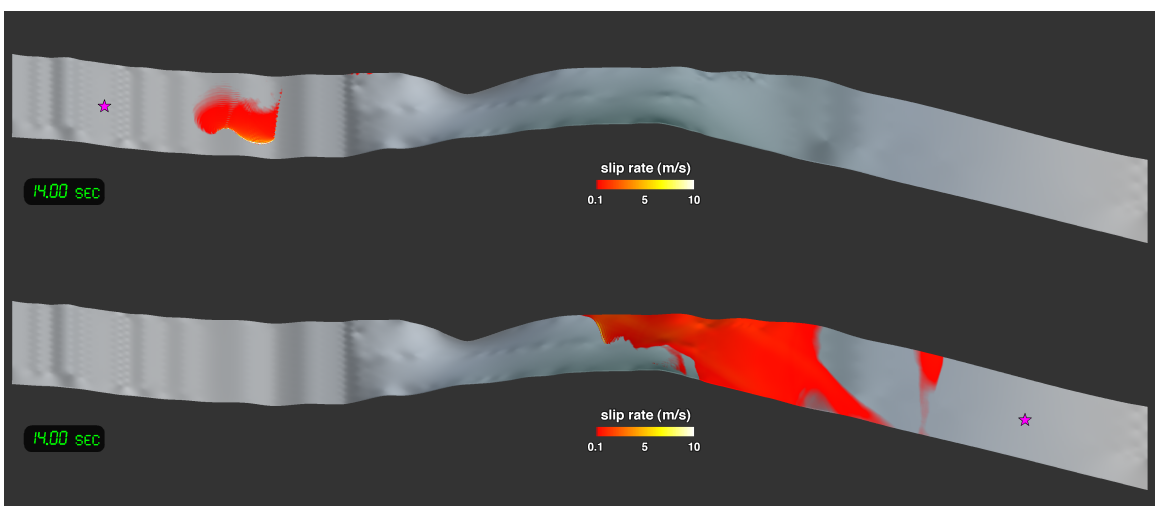

Figure 5. From Simulation Set I: snapshots of slip rates at t = 14 sec from simulations with nucleation centers (denoted as magenta stars) located at (top) the northern SB segment and (bottom) the southern CV segment, respectively. Both ruptures cannot propagate through the SGP.

For the Simulation Set II the initial shear and normal tractions are assigned directly, ignoring the geometrical properties of the fault. The ratio profile between the initial shear traction T_s and normal traction T_s is self-similar (Fig. 6) [*Andrews and Barall*, 2011]. By doing so we implicitly assumed the existence of a heterogeneous

volumetric stress field that is consistent with the initial traction profile.

As shown in Fig. 7, regardless of the nucleation location, the dynamic rupture can go through the middle SGP section with very little perturbation. We also performed comparison calculations with a planar fault using otherwise the same model parameters (initial tractions). We find that the rupture behavior is very similar to the non-planar fault case. As shown in Figures 8 and 9, the rupture front speeds in both the planar and non-planar cases are very close to each other except around the extreme curvature at shallow depth around x_1 = 80 km. This indicates that the rupture does not feel the presence of the geometric irregularities of the scale and smoothness assumed in this simplified fault model since we disregarded the fault geometry by directly assigning initial fault in this case.

To sum up, the fault geometry exhibits two distinctly different roles regarding the plausibility of through-going rupture in the SGP region with the employed model parameters. First, with homogeneous volume stress input and off-fault plasticity, rupture fails to break through the SGP section regardless of propagation direction or speed. In this case, fault geometry dictates the prestress/traction on the fault and has a major effect on rupture dynamics. Second, with heterogeneous fault tractions and pure elasticity, rupture properties do not seems to be affected much by the relatively long-wavelength geometric irregularities of the Banning fault as is represented in the CFM-v4. In this case, fault geometry has very little effect on rupture dynamics. The ground motion patterns in this second case, nevertheless, still shows strong influences from the complex curved fault geometry (Figure 10).

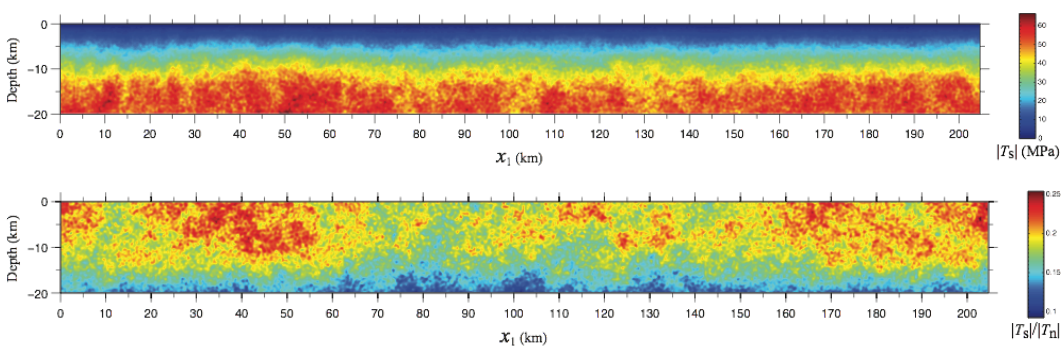

Figure 6. From Simulation Set II: (top) initial shear traction T_s and (bottom) ratio of initial shear traction to initial normal traction $|T_s|/|T_n|$.

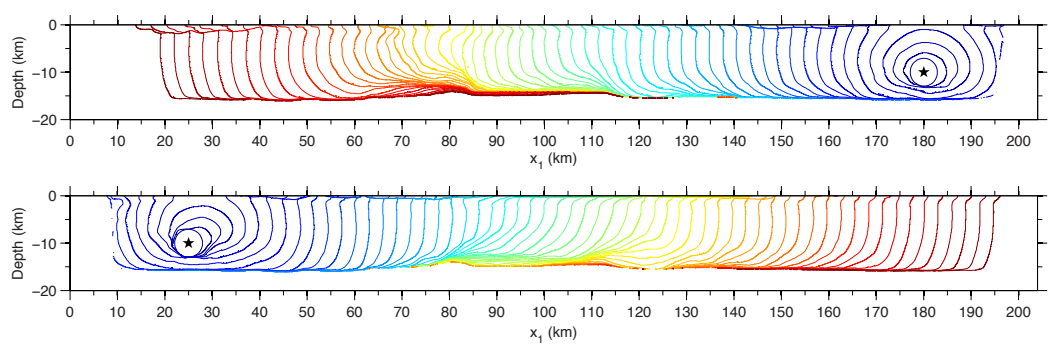

Figure 7. From Simulation Set II: contours of rupture fronts from simulations with nucleation centers located on (top) the northern SB segment and (bottom) the southern CV segment.

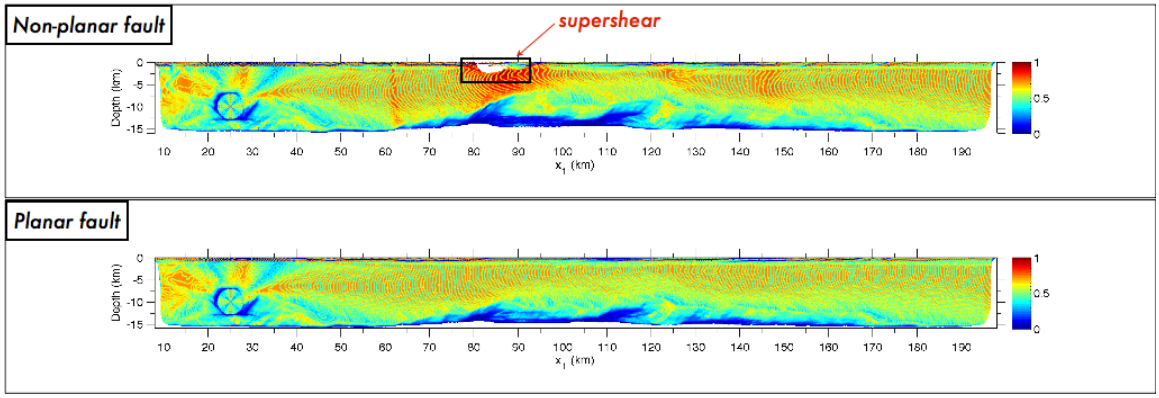

Figure 8. From Simulation Set II: contours of rupture front speeds from simulations nucleated from the north with (top) non-planar fault geometry shown in Fig. 3b and (bottom) planar fault geometry (but with the same initial fault tractions).

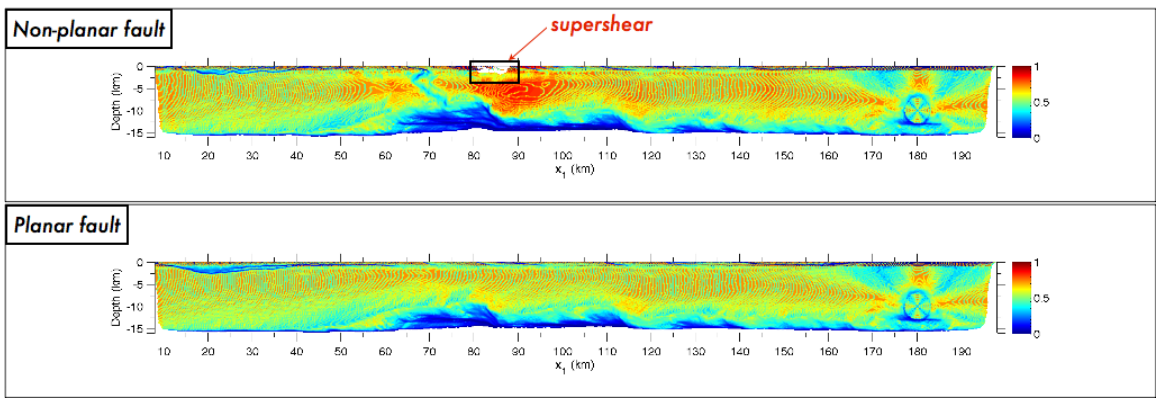

Figure 9. From Simulation Set II: contours of rupture front speeds from simulations nucleated from the south with (top) non-planar fault geometry shown in Fig. 3b and (bottom) planar fault geometry (but with the same initial fault tractions).

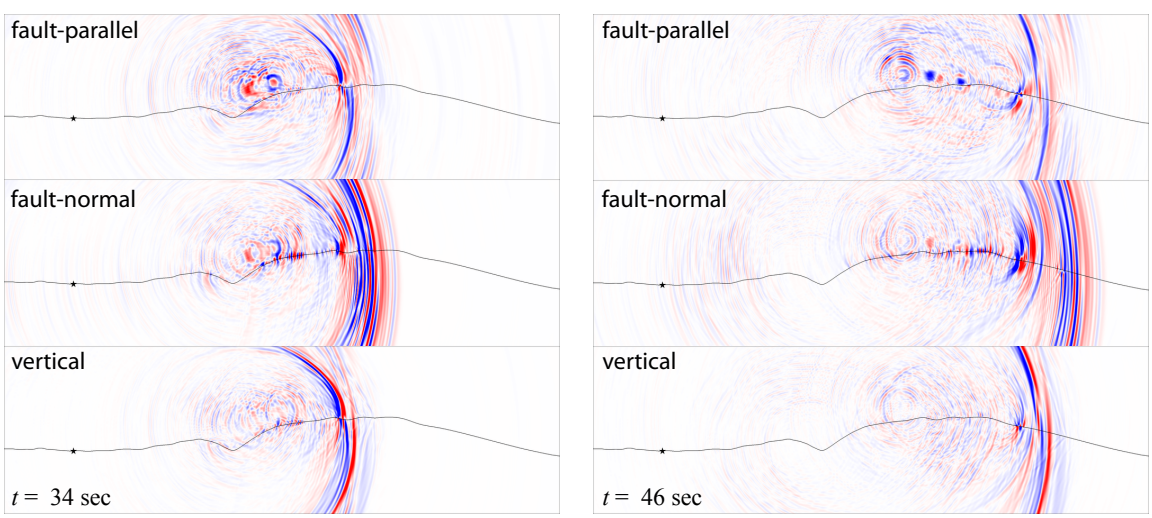

Figure 10. From Simulation Set II: three-component ground acceleration fields at time t = 34 and 46 sec from a rupture event nucleated on the northern SB segment.

Initial fault traction conditions on fault play a very important role in affecting whether or not the rupture can propagate through the SGP, which are, however, poorly constrained. The two end-member cases in our project show distinctly different rupture scenarios. This uncertainty is likely larger than that in the fault geometry. Future work that can provide good constraints on the stress conditions near the SGP will help find a definitive answer to the physical plausibility of through-going rupture along the SGP region of the SAF.

References:

Andrews, D. J., and M. Barall (2011), Specifying initial stress for dynamic heterogeneous earthquake source models, Bull. Seismol. Soc. Am., 101, 2408–2417, doi:10.1785/0120110012.

Ely, G. P., S. M. Day, and J.-B. H. Minster (2009), A support-operator method for 3-D rupture dynamics, Geophys. J. Int., 177(3), 1140–1150, doi:10.1111/j.1365-246X.2009.04117.x.

Ely, G. P., S. M. Day, and J.-B. H. Minster (2010), Dynamic rupture models for the southern San Andreas Fault, Bull. Seismol. Soc. Am., 100(1), 131–150, doi:10.1785/0120090187.

Plesch, A. and others (2007), Community Fault Model (CFM) for southern California, 97, 1793-1802.

Shi, Z., and S. M. Day (2013), Rupture dynamics and ground motion from 3-D rough-fault simulations, J. Geophys. Res., 118, 1 – 20, doi:10.1002/jgrb.50094.

Townend, J., and M. D. Zoback (2004), Regional tectonic stress near the San Andreas fault in central and southern California, Geophys. Res. Lett., 31, L15S11, doi:10.1029/2003GL018918.